Thermodynamics of an idealized hydrologic cycle

Alexandra G. Konings,[1] Xue Feng,[2] Annalisa Molini,[1,2,3] Stefano Manzoni,[1,2]
Giulia Vico,[1,2] and Amilcare Porporato[1,2]

Received 10 August 2011; revised 2 March 2012; accepted 27 March 2012; published 17 May 2012.

[1] The diurnal hydrologic cycle, a sequence of evapotranspiration, boundary layer growth, moist convection, and precipitation, is described in a thermodynamic framework, assuming an atmosphere composed solely of water. This idealized cycle is shown to be equivalent to an abbreviated version of the classical Rankine cycle where not all the water vapor is condensed. Energy and entropy fluxes of the processes involved in the cycle are quantified using the reversible approximation as a function of the quality of the liquid-vapor mixture (the ratio of the residual background vapor and the total mass of water) and the different temperatures at which evaporation and condensation take place. The proposed framework allows quantitative estimates of the net work (which is used by the cycle to drive the atmospheric circulation and dissipated by various frictional forces and nonidealities) as well as of the thermodynamic efficiency of the cycle. Possible extensions of the idealized framework relating to the role of dry air and the inclusion of various irreversible processes are also discussed.

Citation: Konings, A. G., X. Feng, A. Molini, S. Manzoni, G. Vico, and A. Porporato (2012), Thermodynamics of an idealized hydrologic cycle, *Water Resour. Res.*, *48*, W05527, doi:10.1029/2011WR011264.

1. Introduction

[2] The hydrologic cycle coupled to the atmospheric circulation operates as a thermodynamic engine. In particular, the condensation (rainfall) and humidification (evaporation) cycle performs work on the surrounding air, contributing to atmospheric dynamics and ultimately sustaining life on Earth. Solar energy is mainly subdivided into latent and sensible heat fluxes, the first driving evapotranspiration of liquid water from the soil-plant system into the atmosphere and the second causing atmospheric boundary layer (ALB) growth, condensation and moist convection, until precipitation, boundary layer collapse and nighttime cooling repristinate the original conditions. In this manner, radiative energy from the Sun is converted into work that is primarily dissipated by atmospheric circulation but also used in part by ecosystems and humans. As the work done moving water and air throughout the cycle is irreversibly dissipated, with concomitant entropy production [*Tolman and Fine*, 1948], the "engine" operates in conditions of thermodynamic nonequilibrium.

[3] Despite the unavoidable complexities of real processes, classical thermodynamics has demonstrated the great value of using ideal cycles as reference models to quantify and compare the energetics and efficiency of various processes in nature and engineering. In this manner, the well-oiled theoretical and practical machinery of quasi-equilibrium thermodynamics provides useful bounds to maximum efficiency and work achievable compared to real cycles [*Callen*, 1985; *Moran et al.*, 2011]. Irreversible processes can subsequently be added to the picture by methods of linear nonequilibrium thermodynamics [e.g., *Kondepudi and Prigogine*, 1998; *Bejan*, 2006], or by the more ad hoc approach of so-called finite time thermodynamics [*Hoffmann et al.*, 1997].

[4] Entropy and energy budgets have been applied at a range of scales in the Earth sciences, from global entropy budgets (for the entire Earth system using a radiation balance [*Wu and Liu*, 2010] and for the atmosphere alone [*Peixoto et al.*, 1991]) to the thermodynamics of dust devils [*Renno et al.*, 1998]. The thermodynamic budgets of several other components of the Earth system have also been investigated to study their possible consistence with the maximum entropy production (MEP) principle [*Ozawa et al.*, 2003; *Kleidon*, 2009; *Kleidon and Schymanski*, 2008; *Kleidon*, 2010; *Volk and Pauluis*, 2010]. The application of thermodynamic budgets to the water cycle is most relevant in the context of this work.

[5] Working along the lines of classical thermodynamics, *Emanuel* [1988] interpreted hurricane dynamics as a Carnot cycle. Subsequently, *Pauluis and Held* [2002a] argued that the atmosphere acts not only as a heat engine but also as a dehumidifier. In a set of papers [*Pauluis and Held*, 2002a, 2002b; *Pauluis*, 2004], these authors expand on previous entropy balances of moist convection [*Emanuel and Bister*, 1996; *Renno and Ingersoll*, 1996] by adding explicit terms related to the phase of the water in the atmosphere [see also *Goody*, 2003]. The resulting entropy budget was used to calculate the irreversible entropy production due to frictional dissipation and evaporation and diffusion of water vapor. The authors found that these water transport

[1]Nicholas School of the Environment and Earth Sciences, Duke University, Durham, North Carolina, USA.
[2]Department of Civil and Environmental Engineering, Duke University, Durham, North Carolina, USA.
[3]Water and Environmental Engineering Program, Masdar Institute of Science and Technology, Abu Dhabi, United Arab Emirates.

0043-1397/12/2011WR011264

processes account for a significant fraction of the work produced by the atmosphere. As a result, the transport of moist air between areas of different temperature and humidity can be seen as a key thermodynamic function of the atmosphere.

[6] Building upon such prior contributions, in this paper we describe the energy and entropy budget of a simplified hydrological cycle, showing how it is related to the classical thermodynamic cycle of Rankine [e.g., *Moran et al.*, 2011; *Reynolds and Perkins*, 1970; *Bejan*, 2006]. Within this framework, we explore the effect of variations in temperature and the amount of available water on the efficiency of the cycle and on the energy transfers associated with each stage of the cycle. The hydrologic cycle used in this paper is highly idealized: the ideal gas model is used to describe all vapor transformations, liquid water is assumed incompressible, the exact movement of water within the land surface is not modeled, and no sources of irreversibility are included. Each process is treated as quasi-static, such that the cycle is composed of a sequence of equilibrium states. In order to focus on the role of the hydrologic cycle, rather than on the atmospheric dynamics that would be involved in a system with dry air, the atmosphere will be assumed to be composed solely of water vapor. As will be discussed, this not only removes the irreversibility associated with the mixing process, but also allows for neglecting the heat and work fluxes undergone by the dry air while the hydrologic cycle takes place. Such an idealization is equivalent to assuming a hypothetical partitioning of the incoming radiation energy to drive in parallel the water and dry-air cycles, respectively. While in reality the two cycles of dry air and water are highly intertwined, this simplification makes it possible to achieve analytical results that describe clearly the energetics of the hydrologic cycle. We will return to the meaning and limitations of these simplifications, and discuss subsequent steps that may be taken to make the analysis more realistic.

[7] The idealized hydrologic cycle described here can be interpreted as representing the daily evolution of the atmospheric boundary layer, in which energy and moisture fluxes from the land surface expand and condense during the course of the day, triggering the occurrence of convective rainfall in the afternoon. While such processes depend in a complex way on free atmospheric forcing conditions [*Konings et al.*, 2010] and land surface cover [*Juang et al.*, 2007], and are thus highly heterogeneous in space and time, we assume here for simplicity that the cycle repeats itself deterministically with no spatial variability. As a first approximation, infiltration, runoff and the other subsurface components of the hydrologic cycle are also neglected, as they are less important from a thermodynamic point of view.

[8] The rest of the paper is organized as follows. Section 2 defines each of the processes in the cycle, while section 3 discusses the resulting cycle efficiency, the relative sizes of fluxes associated with different processes, and the interpretation of the thermodynamic cycle in the context of the simplifications made. The parallel with the classical thermodynamic theory of heat engines allows us to describe how the hydrologic cycle uses the heat input, and to quantitatively evaluate the role of additional irreversible processes in reducing the efficiency of the cycle. Last, section 4 discusses the role of model assumptions such as neglecting dry air and ice formation, mixture quality, and reversible thermodynamics.

2. Cycle Description

[9] The system under examination consists of a given mass of water m_t undergoing a thermodynamic cycle, and is thus closed to mass exchanges (entrainment and advective fluxes) but open to energy flows from and to the surroundings. Note that when calculating these masses on the basis of observation, it is easiest to do so per unit ground area. The cycle operates between two temperatures T_h and T_c, where $T_h > T_c$, and consists of five processes (illustrated in Figure 1a): $1 \rightarrow 2$, evaporation at constant temperature and pressure; $2 \rightarrow 3$, isothermal expansion of vapor; $3 \rightarrow 4$, adiabatic expansion of vapor; $4 \rightarrow 5$, condensation at constant temperature and pressure; $5 \rightarrow 1$, diabatic compression of liquid and vapor at constant quality.

[10] We assume that in $1 \rightarrow 2$ all the liquid water is evaporated with no liquid residuals, while condensation $4 \rightarrow 5$ may leave a residual part of vapor, m_g^*, which thus always remains as background vapor throughout the cycle. The asterisk denotes conditions of the water mixture in which liquid and vapor coexist. The ratio of this residual to the total water gives the quality of water after condensation,

$$x = \frac{m_g^*}{m_t}, \tag{1}$$

or in terms of the amount of liquid water after condensation, m_l^*,

$$x = 1 - \frac{m_l^*}{m_t}, \tag{2}$$

such that

$$m_g^* = x m_t \quad \text{and} \quad m_l^* = (1 - x) m_t. \tag{3}$$

The cycle starts with a given initial system quality and ends at the same quality.

[11] Figure 1b shows the temperature-entropy (T-s) diagram of the hydrologic cycle studied here, representing the combinations of temperature and specific entropy s (e.g., per unit mass) that the system undergoes during the cycle. T-s diagrams are commonly used in the engineering thermodynamics literature to summarize the behavior of a cycle. The area enclosed by the cycle represents the net work produced. Labeled points correspond to the states between which the processes listed above act. Also shown is the so-called vapor dome, which delineates under what conditions liquid and vapor can coexist: below the vapor dome, water exists as a mixture of liquid and vapor phases; to the right of the vapor dome, only vapor is present, while only liquid is present to the left. The system quality can never decrease to $x = 0$ since there is always residual water vapor present in the atmosphere. As discussed in detail in section 3, this idealized hydrologic cycle corresponds to an "abbreviated" Rankine cycle, a cycle commonly used to describe steam engines. The changes in T and s and the associated energy fluxes are further discussed below for the sequence of processes of this cycle. The symbols used are summarized in Table 1.

2.1. Evaporation ($1 \rightarrow 2$)

[12] The cycle is assumed to start at state 1 with a mass of vapor m_g^* and a mass of liquid m_l^*, quality x, and temperature T_h. The system then undergoes complete quasi-static

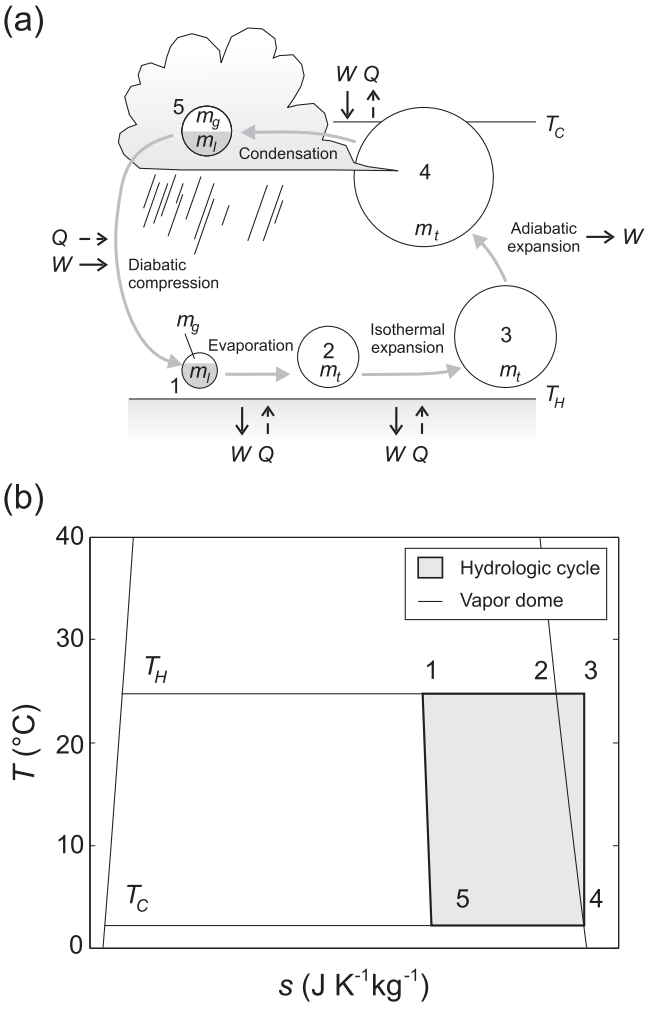

Figure 1. Hydrologic cycle abbreviated as an idealized Rankine cycle: (a) conceptual model and (b) corresponding temperature-entropy diagram. In Figure 1a the thermodynamic quality (ratio of liquid water present to total water) of each process is illustrated qualitatively by the proportion of gray to white areas at each step. The signs of the thermodynamic fluxes associated with each process are also indicated. In Figure 1b the labeled points represent the main states defining the end point of each process (section 2). The thin gray line represents the so-called vapor dome, delineating the areas in which water is present in different phases. Below the vapor dome, the quality of the mixture at a given temperature is determined by the fractional distance between the left ($x = 1$) and the right ($x = 0$) arms of the vapor dome.

evaporation of m_l^* to state 2. This phase of the cycle mimics the continuous evaporation of moisture from the land or ocean surface into the atmosphere that starts after sunrise. Surface evaporation is obtained by letting the initial quantity of liquid m_l^* fully evaporate at constant temperature T_h and pressure equal to the saturation pressure of water, $p^*(T_h)$, given by the Clausius-Clapeyron equation, such that all the water mass is in the vapor state at the end of this process. The value of T_h reflects a typical surface temperature, and is taken as 25°C in the example calculations

Table 1. List of Symbols

Symbol	Description	Units
m_l^*	Mass of liquid after condensation	kg m^{-2}
m_g^*	Mass of gas after condensation	kg m^{-2}
m_t	Total mass of water	kg m^{-2}
p	Water vapor pressure	Pa
p^*	Saturated vapor pressure	Pa
R	Ideal gas constant	J K^{-1} kg^{-1}
W	Work	J m^{-2}
Q	Heat flux	J m^{-2}
S	Entropy	J K^{-1} m^{-2}
s	Specific entropy (per unit mass)	J K^{-1} kg^{-1}
T_h	Hot operating temperature	°C
T_c	Cold operating temperature	°C
U	Internal energy	J m^{-2}
x	Quality of water mixture after condensation	
x_c	Quality of water mixture at maximum efficiency	
ν_l	Specific volume of liquid	m^3 kg^{-1}
c_p^l	Specific heat capacity of liquid water at constant pressure	J K^{-1} kg^{-1}
c_p^g	Specific heat capacity of water vapor at constant pressure	J K^{-1} kg^{-1}
c_v^l	Specific heat capacity of liquid water at constant volume	J K^{-1} kg^{-1}
c_v^g	Specific heat capacity of water vapor at constant volume	J K^{-1} kg^{-1}
η	Efficiency	
λ	Latent heat of vaporization	J kg^{-1}

below. After moving through the surface layer, the resulting water vapor becomes part of the atmospheric boundary layer. Within this simplified framework, the total water vapor available after evaporation makes up the entire ABL.

[13] Evaporation of all the liquid requires a heat input,

$$Q_{12} = m_l^* \lambda(T_h), \tag{4}$$

carrying an (integrated) entropy flux [*Kondepudi and Prigogine*, 1998, p. 130],

$$S_2 - S_1 = \Delta S_{12} = \frac{m_l^* \lambda(T_h)}{T_h}, \tag{5}$$

where $\lambda(T)$ denotes the latent heat of evaporation at temperature T. As a result of evaporation, the system expands, doing work on the surroundings. Since the work is performed against a constant external pressure, it can be calculated as

$$W_{12} = -p^*(T_h)\Delta V_{12} = -m_l^* p^*(T_h)\left[\frac{RT_h}{p^*(T_h)} - \nu_l\right], \tag{6}$$

where ν_l is the specific volume (volume per unit mass) of liquid water. Because the liquid is assumed incompressible, ν_l is independent of T and p.

[14] One can immediately see that the first law of thermodynamics, which for this transformation is $U_2 - U_1 = \Delta U_{12} = Q_{12} + W_{12}$, is satisfied by combining equations (4) and (6). In fact, λ is the change in enthalpy per unit mass of vapor during the change of phase, $\lambda = \Delta u + p^* \Delta \nu$, where lowercase symbols indicate specific quantities (see *Emanuel* [1994, p. 114]; note the different sign convention for work therein). When combined with equation (6) and referred to the mass m_l^*, this expression immediately returns the first law.

2.2. Isothermal Expansion (2 → 3) and Adiabatic Expansion (3 → 4)

[15] After entering the atmosphere by evaporation, the vapor heats and expands as the ABL grows during the early and central part of the day through a complex process driven by a fraction of the radiation energy input. This process is conveniently approximated here as two-stage sequence, comprising first an isothermal expansion, process 2 → 3, followed by an adiabatic one, process 3 → 4. This sequence leads to state 4 of saturated vapor, which is ready to condense as rainfall at the lower temperature T_c (Figure 1).

[16] The evolution of the ABL over the course of the day is accompanied by a vertical temperature profile, which is in contrast with the requirements of classical thermodynamic approaches of a unique temperature at each step. To circumvent this problem, the change in temperature of the ABL over the course of the day is treated as an adiabatic expansion. Although in reality this adiabatic expansion occurs at overlapping times with the isothermal expansion, the two processes are considered separately. They are the result of the cumulative expansion of several parcels as they undergo buoyant rise and adjust adiabatically to the mean temperature profile of their surroundings. This temperature profile is influenced by the thermodynamic properties of the atmosphere surrounding the system air column and its influence on the expansion of individual parcels is therefore not accounted for in process 2 → 3.

[17] Although radiative heating provides most of the heat flux to the ABL over the course of the day, energy and mass may also be transferred because of lateral advection and entrainment flux from above the ABL. However, these fluxes are generally only a relatively small fraction of the surface flux and are neglected here [*Garratt*, 1992; *Porporato*, 2009], so that the cycle can be assumed to be closed with respect to mass exchanges. We will assume that only the upper part of the ABL is cold enough at the end of the daily ABL growth to condense at temperature T_c and form rainfall. In order to ensure that condensation occurs only when rainfall is formed (in step 4 → 5), the combination of steps 2 → 3 and 3 → 4 must therefore raise the specific entropy of the water from that of saturated vapor at T_h to that of saturated vapor at T_c (note that the entropy of vapor decreases with increasing temperature while moving along the Clausius-Clapeyron curve because the increase in pressure has a larger negative effect on the ideal gas entropy than the positive one because of increase in temperature; see also equations (B6) and (B7)).

[18] Since step 3 → 4 occurs adiabatically and therefore isoentropically (as the process is assumed to be reversible), the required increase in specific entropy must occur during the isothermal expansion step. That is $\Delta S_{24} = \Delta S_{23}$ because $\Delta S_{34} = 0$. ΔS_{24} is proportional to the difference between the specific entropy (indicated by s) of saturated vapor at T_h and that at T_c, respectively. Therefore, we can calculate this quantity as [*Moran et al.*, 2011, p. 289]

$$\Delta S_{23} = \Delta S_{24} = m_t(s_4 - s_2) = m_t\left[\int_{T_h}^{T_c} \frac{c_p^g(T)}{T} dT - R\int_{p^*(T_h)}^{p^*(T_c)} \frac{dp}{p}\right], \tag{7}$$

where $c_p^g(T)$ is the temperature-dependent specific heat capacity of water vapor at constant pressure. The pressure at the end of the expansion process can be determined by noting that ΔS_{23} must also equal the change in entropy associated with an isothermal pressure drop from initial pressure p_2 to final pressure p_3, given by $\Delta S_{23} = -R\ln\left(\frac{p_3}{p_2}\right)$ [*Moran et al.*, 2011, p. 290]. Rearranging this expression,

$$p_3 = p^*(T_h)\exp\left(-\frac{\Delta S_{23}}{R}\right), \tag{8}$$

where $p_2 = p^*(T_h)$ is the saturated vapor pressure at temperature T_h. This entropy flux is associated with a heat flux [*Kondepudi and Prigogine*, 1998, p. 79; *Moran et al.*, 2011, p. 282]

$$Q_{23} = T_h \Delta S_{23}. \tag{9}$$

Because process 2 → 3 is isothermal and the vapor is assumed to behave as an ideal gas, the internal energy of the system does not change during this process. It follows immediately from the first law that the work done by the system balances the incoming heat flux. The work can separately be calculated using the familiar expression for isothermal expansion,

$$W_{23} = m_t R T_h \ln\left(\frac{p_3}{p^*(T_h)}\right), \tag{10}$$

which can be simplified to equal equation (9).

[19] In process 3 → 4, the system expands from p_3 to $p^*(T_c)$. Because the expansion occurs adiabatically, no heat flux or associated entropy change takes place. The energy change due to the work of expansion can therefore be calculated simply by evaluating the change in internal energy U between the initial and final temperature. This can be found as [*Kondepudi and Prigogine*, 1998, p. 44; *Moran et al.*, 2011, p. 130]

$$W_{34} = \Delta U_{34} = m_t \int_{T_h}^{T_c} c_v^g(T) dT, \tag{11}$$

where $c_v^g(T)$ is the temperature-dependent specific heat capacity of water vapor at constant volume.

2.3. Condensation (4 → 5)

[20] In process 4 → 5, the vapor is partly condensed at temperature T_c and constant pressure $p^*(T_c)$ until the system is once again at the starting quality x. This process can be thought of as the precipitation-formation process and is associated with an energy release and entropy flux out of the system, respectively computed as

$$Q_{45} = -m_l^* \lambda(T_c) \tag{12}$$

$$\Delta S_{45} = -m_l^* \frac{\lambda(T_c)}{T_c}. \tag{13}$$

Similarly to equation (6), the work performed on the system is given by

$$W_{45} = -m_l^* p^*(T_c)\left(\nu_l - \frac{RT_c}{p^*(T_c)}\right). \tag{14}$$

[21] The temperature T_c should be interpreted as a representative cloud temperature at which most of the condensation and rainfall formation takes place, in the absence of any freezing effect. The limitations related to the assumption of a single representative lower temperature T_c will be discussed in section 4.3.

2.4. Diabatic Compression at Constant Quality (5 → 1)

[22] The last process in the cycle approximates the sequence of transformations between precipitation (and the associated collapse of the ABL) and the following early morning. Through these transformations, the residual vapor and the liquid precipitation are brought down to the surface and warmed back up to T_h. This is clearly a complex sequence which can only be approximately captured by a simple quasi-equilibrium transformation. As a first approximation, it is assumed that all the liquid is restored to its initial conditions by diabatic heating from temperature T_c and pressure $p^*(T_c)$ to the starting temperature T_h and its associated saturation pressure $p^*(T_h)$, requiring a net change of internal energy. The background atmospheric water vapor is also recompressed after rainfall and during nighttime, eventually returning to its starting temperature.

[23] Any reevaporation of precipitation is assumed to be included in process 4 → 5, and all surface evaporation is assumed to occur during process 1 → 2 (i.e., during the day). Thus, the heating 5 → 1 is assumed to occur without any changes of phase and therefore at constant quality. That is, the vapor component of the system is heated and compressed along the saturation curve, an approximation that allows substantial simplification without losing much of the underlying physics. This constant quality assumption defines a unique diabatic heating process. Any potential changes of phase outside of precipitation and land surface evaporation are likely to have only a small effect, as further discussed below.

[24] The compression taking place in 5 → 1 requires work to be done on the system. The necessary work is derived in Appendix A and reads

$$W_{51} = -m_g^* \int_{T_c}^{T_h} \left(R - \frac{\lambda(T)}{T} \right) dT. \tag{15}$$

Since $\frac{\lambda(T)}{T} \gg R$, W_{51} is always greater than zero, as expected. Conversely, there is no work associated with the liquid component as the water is assumed to be incompressible. The required heat input can then be most easily calculated using the first law as

$$Q_{51} = \Delta U_{51} - W_{51} = \int_{T_c}^{T_h} \left\{ m_l^* c_v^l(T) + m_g^* \left[c_v^g(T) + R - \frac{\lambda(T)}{T} \right] \right\} dT, \tag{16}$$

and the entropy flux follows directly as

$$\Delta S_{51} = \int_{T_c}^{T_h} \left\{ \frac{m_l^* c_v^l(T)}{T} + m_g^* \left[\frac{c_p^g(T)}{T} - \frac{\lambda(T)}{T^2} \right] \right\} dT, \tag{17}$$

where the identity $c_v^g + R = c_p^g$ was used. The energy balance associated with the vapor component of the system (i.e., all but the first term in equations (16) and (17)) is such that the work done to compress the water vapor along the saturation curve is greater than the increase in internal energy associated with the increase in temperature. Thus, heat is released from the vapor component. The overall sign of Q_{51} depends on the value of the quality. At low qualities, the energy balance for this process is dominated by the heat input required to return the liquid rainfall to its original temperature, hence $Q_{51} > 0$. At high qualities, the energy balance is dominated by the heat released when compressing (and warming up) the water vapor, thus $Q_{51} < 0$. In the hydrologic cycle, the heat released from compression of the water vapor corresponds to the heat released as radiative cooling by the atmospheric water vapor when the boundary layer collapses and during the stable boundary layer conditions at night. Thus, this heat release from the water vapor is greater than the heat flow into the liquid water phase (during and after infiltration) only when the amount of atmospheric water vapor is sufficiently high (i.e., the quality is sufficiently high).

[25] The change of sign in Q_{51} can also be illustrated by noting that $Q_{51} = \int_{S(T_c)}^{S(T_h)} T dS$. On a T-s diagram, such as that shown in Figure 1b, the diabatic heating process closing the cycle follows a line of constant quality. Such lines interpolate between the saturation curve for fully liquid systems (the left part of the vapor dome, for which $\frac{\partial S}{\partial T} > 0$) and the saturation curve for fully gaseous systems (the right part of the vapor dome, for which $\frac{\partial S}{\partial T} < 0$). The curvature of any given constant quality line depends on the curvature of the liquid and vapor saturation curves, as well as the quality itself. Figure 2a shows the constant quality line for several values of quality. As quality increases, the average $\frac{\partial S}{\partial T}$ along the constant quality line changes from positive to negative, and therefore Q_{51} changes from positive to negative as well. Appendix B derives a formula for the critical quality, x_c at which $Q_{51} = 0$ and $\Delta S_{51} \approx 0$. When numerically evaluated with temperature values typical of the hydrologic cycle, $x_c \approx 0.38$.

2.5. Summary of the Cycle

[26] Table 2 summarizes the cycle states, while Table 3 details the total energy and entropy fluxes into and out of the system during each process. Summing the Q and W columns of Table 3 and treating the liquid as incompressible, we can use $\lambda(T_h) - \lambda(T_c) = \int_{T_c}^{T_h} (c_p^g - c_v^l) dT$ (i.e., Kirchoff's equation [*Emanuel*, 1994, p. 115]) and the definitions of c_p and c_v, as well as $c_v^g + R = c_p^g$, to show that the energy balance of the complete cycle is exactly equal to zero. Using the same Kirchoff's equation and the Clausius-Clayperon relation (equation (A3)), we can further show that the entropy balance closes over this cycle.

[27] The temperature dependence of c_p, c_v, and λ forces numerical evaluation of the energy and entropy fluxes listed in Table 3. Analytical expressions for these fluxes can be obtained by assuming constant values of these parameters as temperature changes (Table 3). With parameters typical of the hydrologic cycle, the differences between the fluxes and efficiencies obtained by the numerical solutions of the integrals and the analytical estimates do not differ significantly. As shown in Figures 2b and 4c, the latter therefore provide valuable approximations to the full model presented in the rest of the paper. Note that the key

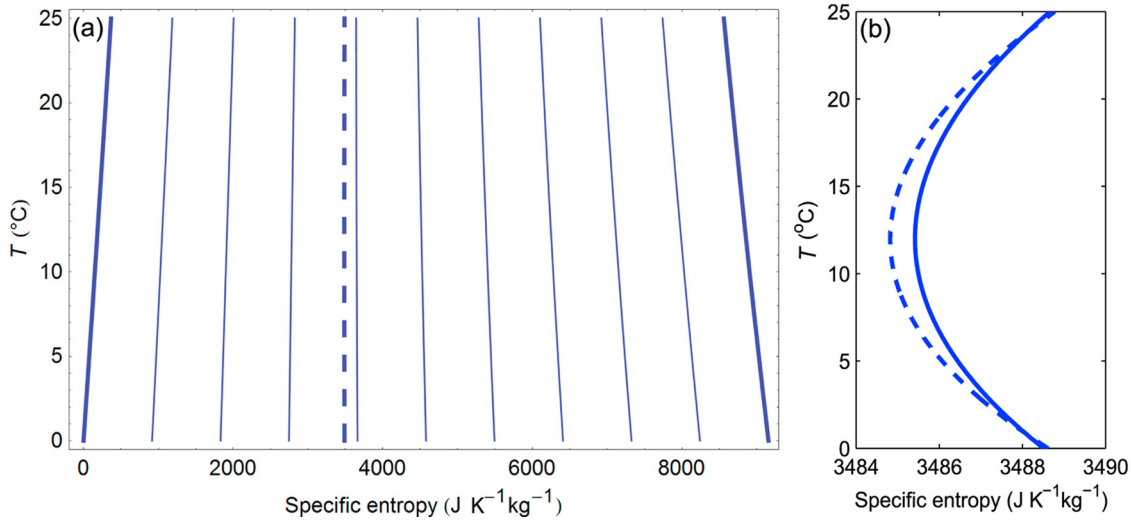

Figure 2. (a) T-s diagram corresponding to constant quality lines from $x = 0$ to $x = 1$ (from left to right) at 0.1 intervals. The thick lines refer to an all-liquid ($x = 0$) or an all-gas ($x = 1$) mixture. The quality for which $\Delta S_{51} = 0$ is shown by the dashed line ($x = x_c \approx 0.38$). (b) Enlarged view of the T-s diagram representing process $5 \rightarrow 1$ for x at $\Delta S_{51} = 0$ (dashed line, analytical solution as calculated in section 2.5; solid line, numerical solution).

assumptions of the model presented in this manuscript (see section 4) apply to both the full numerical and analytical versions.

3. The Hydrologic Cycle as a Modified Rankine Cycle

[28] In the previous description of the hydrologic cycle, we assumed that not all the atmospheric vapor is condensed during the precipitation formation phase, $4 \rightarrow 5$. Hence, in state 5, the system has a finite liquid-vapor mixture quality x. This quality is also kept constant during the transformation $5 \rightarrow 1$, as atmospheric water is only assumed to condense in the context of precipitation formation (i.e., dew formation is neglected), and liquid rainfall is only assumed to evaporate when it leaves the land surface (i.e., reevaporation of rainfall is neglected). Depending on the quality x during $5 \rightarrow 1$, different thermodynamic cycles for water vapor can be investigated (Figure 3). For the extreme case when $x = 1$, no liquid is present at state 5; this case represents the evolution of the atmospheric water vapor without rainfall. The T-s diagram for such a "saturation cycle" is shown in Figure 3 (dotted line). The other extreme is the case in which all the vapor is condensed (i.e., $x = 0$; gray solid line in Figure 3). From an engineering thermodynamics point of view, the latter case corresponds to a Rankine cycle which is used in steam-driven power generation (see *Moran et al.* [2011]; *Reynolds and Perkins* [1970]). Our simplified hydrologic cycle with $0 < x \leq 1$ is an 'abbreviated' Rankine cycle, shown as the "hydrologic cycle" in Figure 3. As will be discussed in section 4.1, typical quality values for the hydrologic cycle are around 0.50–0.70.

Table 2. Summary of Thermodynamic States at Each Stage of the Cycle

State	Quality	m_l	m_g	T	p	V
1	x	m_l^*	m_g^*	T_h	$p^*(T_h)$	$m_l^* \nu_l + m_g^* \frac{RT_h}{p^*(T_h)}$
2	1	0	$m_t = m_l^* + m_g^*$	T_h	$p^*(T_h)$	$\frac{m_t RT_h}{p^*(T_h)}$
3	1	0	m_t	T_h	$p^*(T_h)\exp(\frac{-S_{23}}{R})$	$\frac{m_t RT_h}{p^*(T_h)}\exp\left(\frac{S_{23}}{R}\right)$
4	1	0	m_t	T_c	$p^*(T_c)$	$\frac{m_t RT_c}{p^*(T_c)}$
5	x	m_l^*	m_g^*	T_c	$p^*(T_c)$	$m_l^* \nu_l + m_g^* \frac{RT_c}{p^*(T_c)}$

[29] Step $2 \rightarrow 3$ presents another difference from the Rankine cycle as it is commonly used. When the Rankine cycle is used in steam engines, the water vapor is often superheated (i.e., brought to a temperature greater that the saturation temperature) at constant pressure to a third operating temperature to both increase the efficiency of the whole process and to prevent condensation as the steam passes through the turbine (dashed line in Figure 3). In the case of the hydrologic cycle, however, the "operating" temperatures are limited by the radiative balance of the land surface and lower atmosphere. As a result, instead of superheating at constant pressure, the hydrologic cycle avoids condensation and increases efficiency by 'superheating' at constant temperature, i.e., decreasing pressure.

[30] Figure 3 also shows the hydrologic cycle at the quality for which the "diabatic heating" $5 \rightarrow 1$ occurs with zero net entropy flux, $\Delta S_{51} = 0$, which is further discussed in section 4. In this case, the cycle is very close to a Carnot cycle that includes changes of phase, the so-called wet Carnot cycle [*Moran et al.*, 2011, p. 263].

[31] The use of quasi-equilibrium transformations allows us to compute the efficiency of the hydrologic cycle in converting heat input Q_{in} from solar radiation into net work W_{net} and compare it to the classical efficiencies of the engineering thermodynamic cycles. The W_{net} produced by the hydrologic cycle contributes (along with the work done by the dry air cycle, not considered here) to drive atmospheric

Table 3. Summary of Exact Expressions for the Thermodynamic Fluxes and Analytical Expressions for the Thermodynamic Fluxes Obtained Assuming Constant c_p, c_v, and λ [a]

Process	Q	W	ΔS
		Exact Expressions	
$1 \rightarrow 2$	$m_l^* \lambda(T_h)$	$-p^*(T_h) m_l^* \left(\frac{RT_h}{p^*(T_h)} - \nu_l\right)$	$\frac{m_l^* \lambda(T_h)}{T_h}$
$2 \rightarrow 3$	$T_h \Delta S_{23}$	$-T_h \Delta S_{23}$	$m_t \left[\int_{T_h}^{T_c} \frac{c_p^g(T)}{T} dT - R \int_{p^*(T_h)}^{p^*(T_c)} \frac{dp}{p}\right]$
$3 \rightarrow 4$	0	$m_t \int_{T_h}^{T_c} c_v^g(T) dT$	0
$4 \rightarrow 5$	$-m_l^* \lambda(T_c)$	$-p^*(T_c) m_l^* \left(\nu_l - \frac{RT_c}{p^*(T_c)}\right)$	$-m_l^* \frac{\lambda(T_c)}{T_c}$
$5 \rightarrow 1$	$\int_{T_c}^{T_h} m_l^* c_v^l(T) + m_g^* c_v^g(T) dT - W_{51}$	$-m_g^* \int_{T_c}^{T_h} R - \frac{\lambda(T)}{T} dT$	$\int_{T_c}^{T_h} \frac{m_l^* c_v^l(T)}{T} + \frac{m_g^* c_p^g(T)}{T} - m_g^* \frac{\lambda(T)}{T^2} dT$
		Analytical Expressions	
$1 \rightarrow 2$	$m_l^* \lambda$	$-p^*(T_h) m_l^* \left(\frac{RT_h}{p^*(T_h)} - \nu_l\right)$	$\frac{m_l^* \lambda}{T_h}$
$2 \rightarrow 3$	$T_h \Delta S_{23}$	$-T_h \Delta S_{23}$	$m_t \left[c_p^g \ln \frac{T_c}{T_h} - \lambda \left(\frac{1}{T_h} - \frac{1}{T_c}\right)\right]$
$3 \rightarrow 4$	0	$m_t c_v^g (T_c - T_h)$	0
$4 \rightarrow 5$	$-m_l^* \lambda$	$-p^*(T_c) m_l^* \left(\nu_l - \frac{RT_c}{p^*(T_c)}\right)$	$-m_l^* \frac{\lambda}{T_c}$
$5 \rightarrow 1$	$M(T_h - T_c) - W_{51}$	$-m_g^* \left[R(T_h - T_c) - \lambda \ln \left(\frac{T_h}{T_c}\right)\right]$	$M \ln \left(\frac{T_h}{T_c}\right) + m_g^* \lambda \left(\frac{1}{T_h} - \frac{1}{T_c}\right)$

[a] For simplicity of notation we define $M = m_l^* c_v^l + m_g^* c_v^g$.

circulation and is dissipated by frictional forces (both turbulent winds and drag on falling raindrops) and rainfall drop splashing. The efficiency η of the cycle is given by

$$\eta = \frac{W_{net}}{Q_{in}} = \frac{W_{net}}{Q_{12} + Q_{23} + \vartheta(Q_{51}) Q_{51}}, \tag{18}$$

where $\vartheta(\cdot)$ is the Heaviside step function, used to account for the fact that Q_{51} can be negative for $x < x_c$. The dependences of the individual energy and entropy fluxes and of the efficiency η on quality are shown in Figure 4 for typical values of T_c and T_h. Both the net work and all heat inputs decrease with system quality (except Q_{23}, not shown, which is constant because only vapor is present during process $2 \rightarrow 3$). At low qualities, the total heat input, Q_{in}, decreases faster than the net work, and the cycle efficiency increases with quality. Nevertheless, beyond a certain quality, x_c (which for typical atmospheric conditions is ≈ 0.38; see Appendix B), Q_{51} becomes negative, and as such this flux is no longer an input. As a consequence, Q_{in}

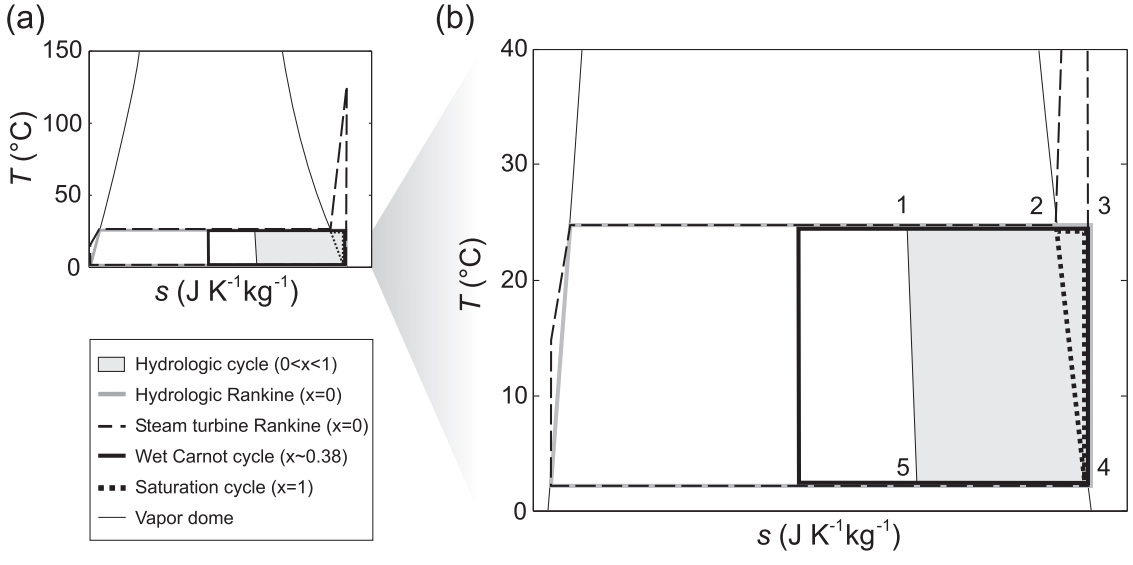

Figure 3. (a) T-s diagrams for the hydrologic cycle (gray shading), its limiting versions at minimum or maximum x (the hydrologic Rankine is shown as a gray line, and the saturation cycle is shown as a black dotted line), the wet Carnot cycle approached when $x = x_c \approx 0.38$ (solid black line), and the equivalent Rankine cycle with constant pressure superheating, as typically used for steam engines (dashed black line). (b) Enlarged view of the T-s diagram to show the details of the hydrologic cycle and its limiting versions.

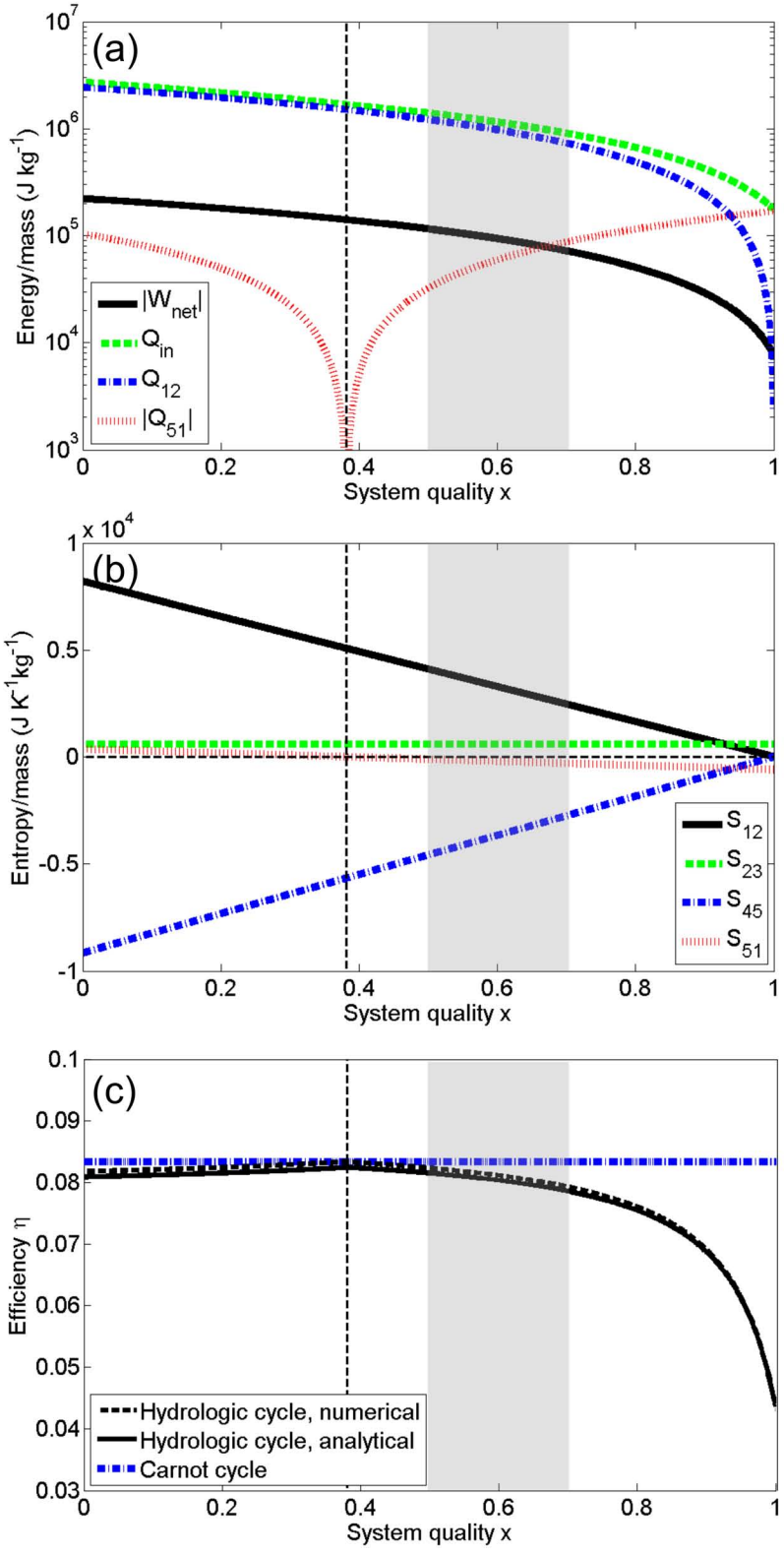

Figure 4. Magnitudes of several components of (a) the energy and (b) entropy balances and (c) efficiency of the modified Rankine cycle as a function of the mixture quality. Shaded areas correspond to a typical quality range for the hydrological cycle. The cycle is assumed to occur between $T_c = 0°C$ and $T_h = 25°C$. In Figure 4c, the solid line represents the analytical solutions, derived by assuming c_v, c_p, and λ are temperature independent, and the dashed line represents the numerical solution. For comparison, the efficiency of a Carnot cycle operating over the same temperature range is also reported (dotted line). The solid point at $x = 0$ in Figure 4c represents the efficiency of a Rankine cycle superheated at constant pressure, rather than at constant temperature, as is commonly done for steam turbines.

decreases less with quality. W_{net} becomes relatively more sensitive to quality, and the total cycle efficiency decreases (Figure 4a). Thus, a maximum efficiency occurs at $x = x_c$, when $Q_{51} = 0$ (Figure 4c). The efficiency remains rather close to the maximum efficiency x_c, up to $x \sim 0.7$, while it quickly declines to much lower values for higher qualities, showing interesting nonlinear behavior of the cycle at quality values near 1.

[32] As discussed in Appendix B, when $x = x_c$ the process $5 \rightarrow 1$ is very close to but not exactly an adiabatic and isoentropic one, as it is associated with small but finite heat and entropy fluxes of opposite signs occurring over the course of the process (that is, $\Delta S_{51} = 0$). The cycle approximately reduces to one containing two sets of alternating isothermal (processes $1 \rightarrow 3$ and $4 \rightarrow 5$) and adiabatic (processes $3 \rightarrow 4$ and $5 \rightarrow 1$) processes, thereby becoming very similar to a wet Carnot cycle (see, for example, *Moran et al.* [2011, p. 263] for a discussion of Carnot cycles that includes a change of phase), with efficiency essentially equal to the Carnot efficiency.

[33] Figure 5a illustrates the dependence of η on T_c and T_h for a set quality, $x = 0.6$ (this value is typical for the hydrologic cycle, as shown in section 4.1). Not surprisingly, the cycle efficiency increases as T_h increases and T_c decreases. The efficiency more than doubles between temperate (e.g., $T_h \approx 10°C$) and tropical climates (e.g., $T_h \approx 27°C$). For this temperature range, the temperature dependence of the cycle efficiency is close to linear, a consequence of the relatively narrow temperature range over which the Earth's climate operates.

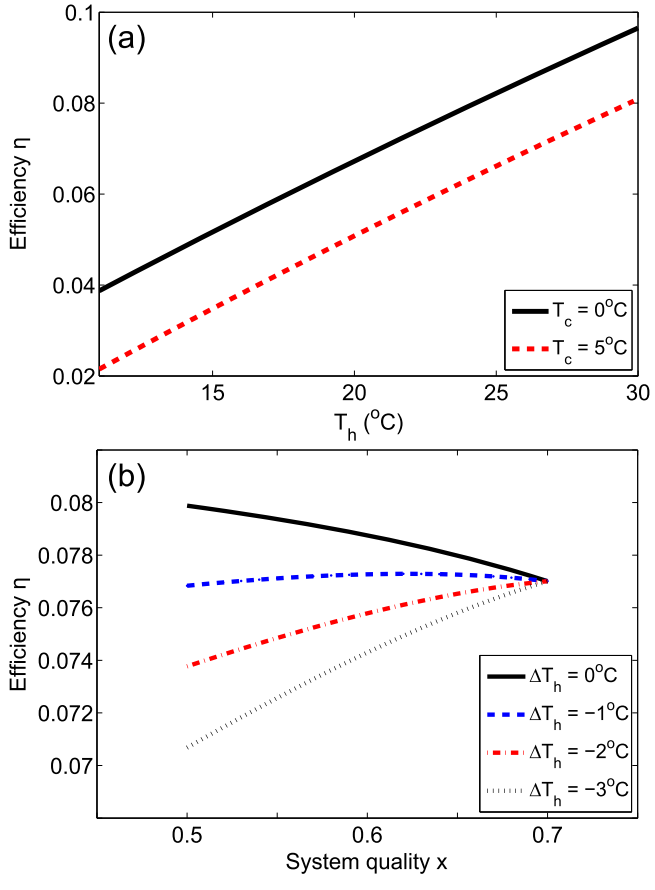

Figure 5. (a) Efficiency of the hydrologic cycle as a function of surface temperature T_h for two different rainfall-generating temperatures T_c. The mixture quality is set at $x = 0.6$. (b) Efficiency as a function of quality for different hypotheses on evaporative cooling, characterized by ΔT_h per $\Delta x = 0.2$.

4. Implications of the Simplifying Assumptions and Possible Extensions

[34] In sections 2 and 3, the hydrologic cycle was mapped onto an abbreviated version of a well-known cycle in engineering thermodynamics, the Rankine cycle. This analogy elucidates the essential processes underlying the sequence of evaporation, boundary layer growth, moist convection and precipitation driving the hydrologic cycle. Our idealization applies more closely to a deterministic repetition of days such as might occur in tropical climates or during certain summer periods in temperate climates. In what follows we discuss the implications of the simplifying assumptions introduced and propose possible extensions of the existing framework to improve realism and facilitate physical interpretations.

4.1. Role of Mixture Quality

[35] Although m_g^* does not contribute to rainfall itself, it contributes to the initiation of rainfall. Increases in m_g^* decrease the height of the lifting condensation level, and make convective rainfall events more likely. The values of m_g^* and x are therefore of interest. Since $m_l^* = m_t - m_g^*$ is equal to the rainfall rate, it is relatively straightforward to estimate. This is not the case for m_g^*, as it is hard to estimate the residual moisture after convective precipitation has ceased. As an alternative, m_g^* may be approximated by assuming that shortly after sunrise evaporation has not yet begun. Therefore, m_g^* equals to the early morning humidity of the air column in the residual ABL. Using a realistic value for the residual ABL height (e.g., ∼1–2 km in the tropics) and assuming a constant dry adiabatic lapse rate of 9.8°C km^{-1} and a hydrostatic atmospheric profile, m_g^* can be estimated. Depending on the initial degree of saturation and surface temperature, m_g^* ranges between ≈15 and 25 kg per unit ground area. Using average rain rates of 5 to 10 mm cycle^{-1} (i.e., 5 to 10 mm d^{-1}), this corresponds to $x \in (0.5, 0.7)$, which is always higher than x_c. The shaded areas in Figure 4 refer to the range of values where the hydrologic cycle typically resides. In this range, both Q_{51} and ΔS_{51} are negative. It is interesting to note that, in terms of efficiency, such estimates of quality place the actual hydrologic cycle within the plateau to the right of the critical threshold (Figure 4c). This suggests that changes in quality alone do not have dramatic consequences on the efficiency and thus points to an overall robustness of the energetics of the hydrologic cycle with respect to changes in quality.

[36] Because the amount of evaporation varies with quality, the amount of evaporative cooling acting to reduce the surface temperature T_h also varies with quality. The approximate role of such cooling can be analyzed as follows. Combining Eqns. (2) and (4) results in a linear decrease of Q_{12} with quality x, where Q_{12} is the latent heat of evaporation. Additionally, consider a simplified surface energy balance in

which the available radiation R is balanced by the sum of latent heat Q_{12} and sensible heat, the latter being proportional to the surface temperature. That is, $R - Q_{12} = g_H(T_h - T_{atm})$, where g_h is aerodynamic conductance, and T_{atm} is a temperature within the atmospheric logarithmic layer. Assuming a T_{atm} proportional to the surface temperature, it follows that surface temperature T_h linearly increases with the quality x. Figure 5b illustrates the effect of different rates of evaporative cooling per change in quality, i.e., for different (constant) values of dT_h/dx. When the rate of cooling is large enough, the reduction of efficiency due to the evaporative cooling overtakes the increase in efficiency due to the increase in quality alone.

[37] Although process 5 → 1 is assumed to take place at constant quality, this is not necessarily the case. If dew formation occurs in the early morning, the system quality will first decrease and then increase (as the dew is evaporated over the course of the day). However, dew formation is likely to impact only a small fraction of the atmospheric water vapor, and thus has only a small effect on the overall fluxes associated with process 5 → 1. Insofar as it does occur, dew formation increases the total efficiency of the cycle. Reevaporation of rainfall may also occur, which would lead to a decrease in system quality between states 5 and 1. Because the cycle is assumed perfectly cyclical, this implies that the amount of condensation was such that the quality at state 5 was lower than that at the start of the cycle (i.e., in the early morning). That is, it would imply that more water was condensed in process 5 → 1 than is evaporated in process 1 → 2.

4.2. The Relative Roles of Water Vapor and Dry Air

[38] The thermodynamic cycle described in this paper does not account for the effect of dry air. In a first approximation, dry air may be considered to undergo a cycle of heating, expansion, cooling, and compression somewhat similar to the water cycle described here, but of course without changes. The cycles for dry air and water may be thought of as taking place in parallel with their own input of incoming radiation energy controlled by the surface energy partitioning (e.g., the Bowen ratio). Each of the two cycles has its own efficiency and nonidealities, but the most striking difference regards their energy use. The hydrologic cycle uses most of the incoming heat to evaporate liquid water during 1 → 2 (Figure 4a). This defines the latent heat flux at the surface. For example, if $m_l^* = 5$ mm d^{-1} (i.e., 5 mm per cycle), $Q_{12} \approx 1.2 \times 10^7$ J m^{-2}. Over a 12 h heating period, the average surface latent heat flux is therefore about 290 W m^{-2}. In contrast, dry air does not exhibit phase changes and uses heat to expand; the work generated during the adiabatic expansion contributes to the instability of the atmosphere. Such expansion is driven by sensible heat fluxes at the surface. Hence, the Bowen ratio can be related to the ratio of the heat input for dry air expansion to the heat input for evaporation in the water cycle, and thus controls the energy partitioning between the two "parallel" cycles.

[39] The idealized hydrologic cycle introduced here is representative of the behavior of local-scale atmospheric water only, with no consideration for large-scale atmospheric motion. Because of the adoption of a closed system, the recycling ratio of our idealized hydrologic cycle, or the fraction of rainfall originating from local evaporation, is exactly one. On a regional scale, recycling ratios are typically estimated to be less than 0.4 [e.g., *Eltahir and Bras*, 1996]. Allowing the recycling ratio to be lower than one and/or to vary would imply opening the system to input and outputs of dry air and water, as well as relaxing the complete cyclicity of the sequence, allowing for days without rainfall and days with rainfall. Opening the system to mass fluxes physically corresponds to considering such factors as entrainment of dry air at the top of the growing boundary layer, or the lateral convection of moisture during cloud convection. *Pauluis* [2011] discusses the work produced by an open cycle representing a segment of a moist atmosphere. His estimates include some irreversibilities associated with entropy production, which result in values of efficiency that are between one sixth and one fifth of the theoretical Carnot maximum for temperatures and humidity values typical of Earth.

4.3. Role of Condensation Temperature and Ice Formation

[40] In the previous analyses, we adopted a single temperature T_c, representative of the cloud temperature at which most of the condensation and rainfall formation take place, and neglected possible ice formation. These assumptions may lead to underestimated efficiencies. In reality, the typical temperatures over which the daily hydrologic cycle acts on a warm day with convective precipitation are between 20°C and 30°C at the surface and –5°C and –15°C at the cloud top, respectively. Condensation takes place at different heights/temperatures and pressures within clouds, so freezing and deposition may occur as well as condensation.

[41] In our idealized hydrological cycle, we can frame the process of ice formation and melting in two ways that are consistent with the classical thermodynamic theory. The two conceptual schemes represent the end members of the continuum between freezing of liquid water and deposition of vapor in absence of liquid. One limit case assumes only liquid water cools and freezes, followed by melting and warming. This process can be considered as a reversible, quasi-static process, which basically involves no net work, equal input and output heat fluxes, and no entropy production. In this case, the hydrologic cycle would therefore not significantly change its efficiency even if it reaches lower temperatures (except through the effect of the small temperature dependence in the latent heat of evaporation). The other limiting case assumes that water vapor is deposited in the absence of liquid water. That is, it assumes the temperature at step 4 is below freezing and no liquid water is formed. This process allows the water to reach lower temperatures in a Rankine-like cycle with deposition (instead of condensation) and therefore results in higher efficiencies (always bounded by the Carnot efficiency; for reference Carnot efficiency is 0.084 when operating between 0°C and 25°C (see Figure 4c), while it rises to 0.12 if the lower temperature is reduced to −10°C).

[42] More likely, vapor is involved in the formation of ice in the presence of supercooled liquid water, especially in water-saturated clouds. In fact, below the freezing point the saturation vapor pressure over ice is lower than over liquid water, so that vapor preferentially deposits on ice while (supercooled) liquid water evaporates [*Jacobson*, 2005]. This is the case for tall cumulus clouds such as those typical

in the tropics, where the cloud temperature can extend well below zero, and water vapor may be deposited to form ice rather than liquid water [*House*, 1993]. Deposition may greatly increase efficiency relative to a scenario without ice formation, as the vapor can then reach much lower temperatures T_c (on the order of $-15°C$) at state 4 of the cycle. In such a scenario, Q_{45} depends on the latent heat of sublimation rather than on the latent heat of evaporation. Depending on the exact cloud dynamics, such ice is frequently remelted or sublimated. The resulting local change in temperature and density affects the buoyancy of air parcels and therefore in turn influences cloud dynamics [*Iribarne and Godson*, 1981; *Dufour and Defay*, 1963]. Such cycles of changes to and from the ice phase can be neglected in the quasi-static limit of the reversible equilibrium thermodynamics. In this limiting scenario, any ice particles formed are assumed to have melted by the time they fall out of the clouds.

4.4. Sources of Irreversibility and Other Nonidealities

[43] The hydrologic cycle described above is made of reversible steps connecting equilibrium states. This approach neglects the intermediate microscopic steps needed to complete each process of the cycle, as well as processes that are inherently irreversible and thus produce entropy [*Tolman and Fine*, 1948; *Kondepudi and Prigogine*, 1998; *Bejan*, 2006]. These introduce inefficiencies in the conversion of thermal radiation into work (e.g., water transport by the hydrologic cycle), so that this idealized description only provides an upper bound to the real efficiency of the hydrologic cycle.

[44] Irreversible entropy production occurs mainly because of frictional dissipation and mixing of dry air and water vapor. The former is related to turbulent dissipation or air flows, drag on falling raindrops and rainfall splashing on the ground (some of these effects were previously described by *Pauluis and Held* [2002a], where it was found that frictional dissipation contributes less to the total entropy budget than the irreversibilities associated with phase changes of water). For the entropy budget, neglecting dry air and the corresponding irreversibilities amounts to neglecting the related entropy production during mixing or demixing with water when a phase change of water occurs without a phase change of dry air (i.e., during evaporation and condensation). However, such an entropy production tends to be relatively small compared to the reversible entropy fluxes. In fact, in a typical atmosphere with a mixing ratio ≈ 0.01, the entropy of mixing between dry air and evaporated water is less than 1% of the entropy of latent heat flux from a phase change.

[45] Finally, because cloud dynamics are not explicitly simulated, several other sources of energy loss are neglected. These include the occurrence of supersaturated air parcels, the possibility of penetrative downdrafts, the effect of turbulence on enhancing drop formation, as well as the reevaporation of condensed droplets, both in the cloud and after falling, and the effects of ice formation.

[46] The so-called finite time thermodynamics [*Hoffmann et al.*, 1997; *de Vos*, 1985; *Bejan*, 2006] provides a relatively simple scheme to go beyond the equilibrium idealization, adding some irreversible components such as conductances and given radiation fluxes to impose a specific time scale for heat transfer into and from the system. A finite time thermodynamic description of the hydrologic cycle would not only allow to sharpen the efficiency estimates of the abbreviated Rankine cycle, but also provide a way to test different hypotheses of operation, e.g., maximum power and entropy production, minimum rate of dissipation, etc. [*Hoffmann et al.*, 1997; *Kleidon and Schymanski*, 2008; *Kleidon*, 2010]. We leave this to further contributions.

5. Conclusions

[47] This paper has analyzed the essential processes contributing to the diurnal hydrologic cycle, from heating and evaporation, to expansion and condensation, to convective rainfall. Using a simplified representation, it was shown that the hydrologic cycle corresponds in its essence to a modified Rankine cycle. The cycle uses heat in the form of radiation from the Sun and water as working fluid and produces work that sustains circulation and liquid vapor transformations essential to the climate and life on Earth. The efficiency of this cycle depends on the mixture quality, or on the partitioning between background atmospheric water vapor and rainfall. For values of quality typical of the Earth system, the cycle efficiency depends on the operating temperatures, increasing with the surface temperature and decreasing with the cloud temperature. The hydrologic cycle is more efficient in tropical climates. The cycle efficiency also decreases as mixture quality increases. In other words, the efficiency increases as more of the total water undergoes phase transformations through precipitation and subsequent evaporation. The maximum efficiency occurs at a quality below the values typical for the Earth system. However, for realistic ranges of quality, the efficiency of the cycle does not change very much. This suggests the energetics of the hydrologic cycle are relatively robust to changes in the quality of the moisture cycle in a given area.

[48] The analysis of the present paper shares many features with the work of *Pauluis* [2011], in which the Carnot cycle was combined with an open cycle representing mass transfer of water that acts as a dehumidifier. While the goal of Pauluis' paper is somewhat similar to ours, the dehumidification engine proposed therein is described as an open system with attention to its effect on the surrounding atmosphere (i.e., by changing the distribution of specific humidity), rather than considering the areally averaged effect of cyclical evaporation and precipitation processes acting across different temperatures. Our contribution focuses on quasi-equilibrium processes of a closed system, and analyzes in detail the thermodynamic processes that water undergoes between the land surface and the atmosphere during the different phases of a diurnal cycle. Hence, it is complementary to the analysis of *Pauluis* [2011]. For example, the efficiency of the cycle presented by *Pauluis* [2011] deviates from the theoretical maximum Carnot efficiency when the moistening (evaporation, in the case of the hydrologic cycle) and drying (precipitation) steps do not occur at saturation. In the model presented in this manuscript, the evaporation and condensation processes always occur at saturation. However, the efficiency generally deviates from the Carnot efficiency because the nighttime collapse of the boundary layer is a diabatic process. In contrast, because *Pauluis* [2011] focuses on local transport of moisture only, the mixed Carnot steam cycle presented therein contains only adiabatic and isothermal processes. In future contributions, we plan to merge the two approaches and analyze them within the context of the diurnal ABL dynamics.

[49] The heat and work associated with the processes of the hydrologic cycle presented here are linked to the heat and work associated with the spatiotemporal evolution of dry air. This evolution has not been specifically incorporated here. Similarly, the effect of ice formation in clouds, or of the production of snow and hail, has been described only as operating between a set of two limiting cases. Nevertheless, the idealization of the hydrologic cycle as a reversible version of an abbreviated Rankine cycle provides a framework for studying the thermodynamic contributions of the water cycle on which more sophisticated representations can be based.

Appendix A: Derivation of W_{51}

[50] The calculation of the work associated with a diabatic heating process at constant quality requires knowing the evolution of either pressure, volume, or temperature. Since the process is defined as taking place between temperatures T_c and T_h at saturation pressure, it is easiest to calculate the integral as a function of temperature as

$$\begin{aligned} W_{51} &= -\int pdV = \int p^*(T)\frac{dV}{dT}dT \\ &= -\int p^*(T)\left(\frac{dV_l}{dT}+\frac{dV_g}{dT}\right)dT \\ &= -\int p^*(T)\left(\frac{dV_l}{dT}+m_g^*R\left[\frac{1}{p^*(T)}-\frac{T}{p^*(T)^2}\frac{dp^*(T)}{dT}\right]\right)dT, \end{aligned} \tag{A1}$$

where $\frac{dV_g}{dT}$ is expanded using the ideal gas law and the chain rule, and $\frac{dV_f}{dT} = m_l\frac{dv_l}{dT}$, with $\frac{dv_l}{dT}$ determined from thermodynamic tables [*Kondepudi and Prigogine*, 1998]. If the liquid is taken to be incompressible, $\frac{dv_l}{dT} = 0$. Simplifying the remaining terms leads to

$$W_{51} = -\int m_g^*R - p^*(T)\frac{m_g^*RT}{p^*(T)^2}\frac{dp^*(T)}{dT}dT, \tag{A2}$$

where $\frac{dp^*(T)}{dT}$ is given by the Clausius-Clapeyron equation as

$$\frac{dp^*(T)}{dT} = \frac{p^*(T)\lambda(T)}{RT^2}. \tag{A3}$$

This leads to

$$W_{51} = -m_g^*\int R - \frac{\lambda(T)}{T}dT. \tag{A4}$$

Appendix B: Conditions Under Which $Q_{51} = 0$ and $\Delta S_{51} \approx 0$

[51] For simplicity, the derivation below is performed per unit mass of the system. Here Q_{51} and ΔS_{51} are determined as a function of $\frac{\partial s}{\partial T}$. Thus, we need to solve

$$\frac{Q_{51}}{m_t} = \int_{T_c}^{T_h} T\frac{\partial s}{\partial T}dT = 0 \tag{B1}$$

$$\frac{\Delta S_{51}}{m_t} = \int_{T_c}^{T_h} \frac{\partial s}{\partial T}dT = 0 \tag{B2}$$

by finding a constant quality x_c for which these expressions are (approximately) verified

[52] We begin by noting that during process $5 \rightarrow 1$, both vapor and liquid phases are present. As a result, s is a weighted average of the specific entropy of liquid $s_l(T)$ and the specific entropy of water vapor $s_g(T)$, i.e.,

$$s(x,T) = s_l + x(s_g - s_l), \tag{B3}$$

from which

$$\frac{ds}{dT} = \frac{ds_l}{dT} + x\left(\frac{ds_g}{dT} - \frac{ds_l}{dT}\right). \tag{B4}$$

If water is treated as an incompressible fluid, $\frac{ds_l}{dT} = \frac{c_p^l(T)}{T}$. Additionally,

$$\frac{ds_g}{dT} = \frac{\partial s_g}{\partial T} + \frac{\partial s_g}{\partial p}\frac{\partial p}{\partial T}. \tag{B5}$$

Using the fact that for an ideal gas $s_g(T,p) = s_g(T_0,p_0) + c_p^g\ln(T/T_0) - R\ln(p/p_0)$ [*Moran et al.*, 2011],

$$\frac{ds_g}{dT} = \frac{c_p^g(T)}{T} - \frac{R}{p}\frac{\partial p}{\partial T}. \tag{B6}$$

Since s_g is at saturation during process $5 \rightarrow 1$, $\frac{\partial p}{\partial T}$ is given by the Clausius-Clapeyron equation (equation (A3)). Substituting and simplifying gives

$$\frac{ds_g}{dT} = \frac{c_p^g(T)}{T} - \frac{\lambda(T)}{T^2}. \tag{B7}$$

Substituting this into equation (B4),

$$\frac{\partial s}{\partial T} = \frac{c_p^l(T)}{T} + x\left[\frac{c_p^g(T)}{T} - \frac{\lambda(T)}{T^2} - \frac{c_p^l(T)}{T}\right]. \tag{B8}$$

Note that because the right-hand side of (B8) depends on temperature, there is no single value of x for which $\frac{\partial s}{\partial T} = 0$ over a range of temperatures.

[53] Equations (B1) and (B2) can then be rewritten as

$$\frac{\Delta S_{51}}{m_t} = 0 = \int_{T_c}^{T_h}\frac{c_p^l(T)}{T} + x\left[\frac{c_p^g(T)}{T} - \frac{\lambda(T)}{T^2} - \frac{c_p^l(T)}{T}\right]dT \tag{B9}$$

$$\frac{Q_{51}}{m_t} = 0 = \int_{T_c}^{T_h} c_p^l(T) + x\left[c_p^g(T) - \frac{\lambda(T)}{T} - c_p^l(T)\right]dT. \tag{B10}$$

[54] Recall that in process $5 \rightarrow 1$, the quality x is constant. Therefore, ΔS_{51} and Q_{51} cannot be zero for the same value of x. Nevertheless, the two are closely related, and there exists a critical quality x_c for which $Q_{51} = 0$ and $\Delta S_{51} \approx 0$. Although the s at a given quality varies with temperature over the transformation from $T = T_c$ to $T = T_h$, the total $\Delta S_{51} \approx 0$. As discussed in section 3.1, when the quality is such that Q_{51} is exactly zero, the cycle

efficiency is maximized. Since $\Delta S_{51} \approx 0$ at this quality, process $5 \rightarrow 1$ is nearly isoentropic and the cycle is very close to a wet Carnot cycle. x_c can be determined by rearranging equation (B10)

$$x_c = \frac{\int_{T_c}^{T_h} \frac{c_p^l(T)}{T} dT}{\int_{T_c}^{T_h} \left(\frac{c_p^l(T)}{T} - \frac{c_p^g(T)}{T} + \frac{\lambda(T)}{T^2} \right) dT}. \quad \text{(B11)}$$

If constant values for c_p^l, c_p^g, and λ are assumed (Table 3, analytical expressions), then the constant quality for which $Q_{51} = 0$ can be obtained analytically as

$$x_c = \frac{1}{1 - \frac{c_p^g}{c_p^l} - \frac{\lambda}{c_p^l \ln(T_h/T_c)} \left(\frac{1}{T_h} - \frac{1}{T_c} \right)}. \quad \text{(B12)}$$

[55] The x_c thus depends on the temperatures T_c and T_h. For $T_c = 0°C$ and $T_h = 25°C$, $x_c = 0.382$. However, for values of T_c and T_h typical of the Earth surface and troposphere, the dependence of x_c on temperature is weak. This can be seen by calculating the qualities $x_c^{lim}(T)$ at which the value of $\frac{\partial s}{\partial T} = 0$ for different temperatures. For $T_c = 0°C$, $x_c^{lim} = 0.37$, while for $T_c = 25°C$, $x_c^{lim} = 0.40$, and increases almost linearly in between.

[56] **Acknowledgments.** The authors gratefully acknowledge valuable discussions with J.R. Rigby and Adrian Bejan. We also thank A. Kleidon and S. Schymanski and two anonymous reviewers for constructive suggestions. The authors were supported by the NSF through the Graduate Research Fellowship program and through grants NSF-CBET-1033467 and NSF-EAR-1063717. This research was also supported by the U.S. Department of Agriculture through grant 2011-67003-30222 and the U.S. Department of Energy through the Office of Biological and Environmental Research (BER) Terrestrial Ecosystem Science (TES) Program (DE-SC0006967).

References

Bejan, A. (2006), *Advanced Engineering Thermodynamics*, 880 pp., John Wiley, Hoboken, N. J.

Callen, H. B. (1985), *Thermodynamics and an Introduction to Thermostatistics*, 493 pp., John Wiley, New York.

de Vos, A. (1985), Efficiency of some heat engines at maximum-power conditions, *Am. J. Phys.*, *53*, 570–573.

Dufour, L., and R. Defay (1963), *Thermodynamics of Clouds, Int. Geophys. Ser.*, vol. 6, 255 pp., Academic, New York.

Eltahir, E., and R. Bras (1996), Precipitation recycling, *Rev. Geophys.*, *34*, 367–378.

Emanuel, K. (1988), The maximum intensity of hurricanes, *J. Atmos. Sci.*, *45*, 1143–1155.

Emanuel, K. A. (1994), *Atmospheric Convection*, 580 pp., Oxford Univ. Press, Oxford, U. K.

Emanuel, K., and M. Bister (1996), Moist convective velocity and buoyancy scales, *J. Atmos. Sci.*, *53*, 3276–3285.

Garratt, J. R. (1992), *The Atmospheric Boundary Layer*, 316 pp., Cambridge Univ. Press, Cambridge, U. K.

Goody, R. (2003), On the mechanical efficiency of deep, tropical convection, *J. Atmos. Sci.*, *60*, 2827–2832.

Hoffmann, K. H., J. M. Burzler, and S. Schubert (1997), Endoreversible thermodynamics, *J. Non-Equilib. Thermodyn.*, *22*, 311–355.

House, J. R. A. (1993), *Cloud Dynamics*, 573 pp., Academic, San Diego, Calif.

Iribarne, J., and W. Godson (1981), *Atmospheric Thermodynamics, Geophys. Astrophys. Monogr.*, vol. 6, D. Reidel, Dordrecht, Netherlands.

Jacobson, M. Z. (2005), *Fundamentals of Atmospheric Modeling*, 2nd ed., 813 pp., Cambridge Univ. Press, Cambridge, U. K.

Juang, J. Y., A. Porporato, P. C. Stoy, M. S. Siqueira, A. C. Oishi, M. Detto, H. S. Kim, and G. G. Katul (2007), Hydrologic and atmospheric controls on initiation of convective precipitation events, *Water Resour. Res.*, *43*, W03421, doi:10.1029/2006WR004954.

Kleidon, A. (2009), Nonequilibirum thermodynamics and maximum entropy production in the Earth system, *Naturwissenschaften*, *96*, 653–677, doi:10.1007/s00114-009-0509-x.

Kleidon, A. (2010), Life, hierarchy, and the thermodynamic machinery of planet Earth, *Phys. Life Rev.*, *7*, 424–460, doi:10.1016/j.plrev.2010.10.002.

Kleidon, A., and S. Schymanski (2008), Thermodynamics and optimality of the water budget on land: A review, *Geophys. Res. Lett.*, *35*, L20404, doi:10.1029/2008GL035393.

Kondepudi, D., and I. Prigogine (1998), *Modern Thermodynamics: From Heat Engines to Dissipative Structures*, 486 pp., John Wiley, New York.

Konings, A. G., G. G. Katul, and A. Porporato (2010), The rainfall-no rainfall transition in a coupled land-convective atmosphere system, *Geophys. Res. Lett.*, *37*, L14401, doi:10.1029/2010GL043967.

Moran, M. J., H. N. Shapiro, D. B. Boettner, and M. B. Bailey (2011), *Fundamentals of Engineering Thermodynamics*, 7th ed., 1004 pp., John Wiley, Hoboken, N. J.

Ozawa, H., A. Ohmura, R. D. Lorenz, and T. Pujol (2003), The second law of thermodynamics and the global climate system: A review of the maximum entropy production principle, *Rev. Geophys.*, *41*(4), 1018, doi:10.1029/2002RG000113.

Pauluis, O. M. (2004), Water vapor and entropy production in the Earth's atmosphere, in *Non-equilibrium Thermodynamics and the Production of Entropy: Life, Earth, and Beyond*, edited by A. Kleidon and R. D. Lorenz, pp. 107–119, Springer, Berlin.

Pauluis, O. (2011), Water vapor and mechanical work: A comparison of Carnot and steam cycles, *J. Atmos. Sci.*, *68*, 91–102, doi:10.1175/2010JAS3530.1.

Pauluis, O., and I. M. Held (2002a), Entropy budget of an atmosphere in radiative-convective equilibrium. Part I: Maximum work and frictional dissipation, *J. Atmos. Sci.*, *59*, 125–139.

Pauluis, O., and I. M. Held (2002b), Entropy budget of an atmosphere in radiative-convective equilibrium. Part II: Latent heat transport and moist processes, *J. Atmos. Sci.*, *59*, 140–149.

Peixoto, J. P., A. H. Oort, M. Dealmeida, and A. Tome (1991), Entropy budget of the atmosphere, *J. Geophys. Res.*, *96*, 10,981–10,981.

Porporato, A. (2009), Atmospheric boundary-layer dynamics with constant Bowen ratio, *Boundary Layer Meteorol.*, *132*(2), 227–240, doi:10.1007/s10546-009-9400-8.

Renno, N. O., and A. P. Ingersoll (1996), Natural convection as a heat engine: A theory for CAPE, *J. Atmos. Sci.*, *53*, 572–585.

Renno, N. O., M. L. Burkett, and M. P. Larkin (1998), A simple thermodynamical theory for dust devils, *J. Atmos. Sci.*, *55*, 3244–3252.

Reynolds, W. C., and H. C. Perkins (1970), *Engineering Thermodynamics*, 585 pp., McGraw-Hill, New York.

Tolman, R. C., and P. C. Fine (1948), On the irreversible production of entropy, *Rev. Mod. Phys.*, *20*(1), 51–77.

Volk, T., and O. Pauluis (2010), It is not the entropy you produce, rather how you produce it, *Philos. Trans. R. Soc. London B*, *365*, 1317–1322.

Wu, W., and Y. Liu (2010), Radiation entropy flux and entropy production of the Earth system, *Rev. Geophys.*, *48*, RG2003, doi:10.1029/2008RG000275.

X. Feng, S. Manzoni, A. Porporato, and G. Vico, Department of Civil and Environmental Engineering, Duke University, Durham, NC 27708, USA.

A. G. Konings, Nicholas School of the Environment and Earth Sciences, Duke University, Durham, NC 27708, USA. (konings@alum.mit.edu)

A. Molini, Water and Environmental Engineering Program, Masdar Institute of Science and Technology, PO Box 54224, Abu Dhabi, United Arab Emirates.